www.czasopisma.pan.pl PAN www.journals.pan.pl
Opto-Electronics Review 27 (2019) 369–377

Contents lists available at ScienceDirect

Opto-Electronics Review

journal homepage: http://www.journals.elsevier.com/opto-electronics review

Full Length Article

Design of a highly sensitive photonic crystal refractive index sensor incorporating ring-shaped GaAs cavity

F. Rahman-Zadeh [a], M. Danaie [b,*], H. Kaatuzian [a]

[a] Photonics Research Lab., Electrical Engineering Department, Amirkabir University of Technology, Tehran, Iran
[b] Electrical and Computer Engineering Faculty, Semnan University, Semnan, Iran

ARTICLE INFO

Article history:
Received 16 April 2019
Received in revised form 3 September 2019
Accepted 25 November 2019
Available online 20 December 2019

Keywords:
Refractive index sensor
Biosensor
Photonic crystal
Label free
Optical resonator

ABSTRACT

Two highly sensitive optical sensor topologies are proposed and simulated in this paper. The proposed structures are optimized to provide better performance characteristics such as sensitivity, detection limit, and quality factor. They are based on two-dimensional photonic crystals consisting of rectangular arrays of GaAs rods in SiO_2 substrates. Such lattices have bandgaps for transverse magnetic modes. Two-dimensional finite difference time domain and plane wave expansion methods are used for the simulation and analysis of the refractive index sensors and particle swarm optimization method is used to optimize the structural parameters. The designed structures show a high sensitivity to refractive index variations. They are able to detect refractive indices from 1.33 to 1.5. An excellent figure of merit equal to 737 RIU^{-1} is observed for the proposed structure and a significant improvement is observed compared to the structures reported in the literature.

1. Introduction

Photonic crystals (PCs) are periodic structures which consist of two different materials, for which the optical properties, i.e. permittivity (ε) or permeability (μ) are modulated by a lattice constant. Such an arrangement can create an optical bandgap. The existence of optical bandgap means that some wavelengths are forbidden to pass through the lattice. PCs have a wide range of applications in many optical systems such as nanolasers [1,2], Mach-Zehnder switches [3], logical gates [4,5], phase detectors [6], spectrometers [7], directional couplers [8,9], and power splitters [10,11].

Refractive index measurement is one of the many methods used for diagnosis of cancerous tissues [12–15]. There are various biosensors designed and fabricated for this purpose using a variety of technologies including piezoelectric [12], carbon nanotube [13], electrochemical [14] methods [15]. Another method that can be used for the implementation of refractive index sensors is through using surface plasmons [16–20]. Although such devices occupy much smaller footprints [20–23], but they have higher absorption values and lower Q-factors than PCs [24,25]. PCs can confine light in ultra-high quality factor cavities. The sensitivity of many PC cavities is usually high enough to sense small changes in refractive indices which can be induced due to concentration changes of the analyte in order of 0.01 of refractive index unit (RIU).

There are many approaches for implementation of refractive index sensors using PCs [13,14]. In Ref. 14 a planar PC waveguide is fabricated using the silicon-on-insulator (SOI) technique. It uses a 250 nm silicon layer on a 3 μm buried oxide layer. A biosensor based on PC L13 cavity (which is created by removing 13 holes in a row) is reported in Ref. 15. It has good features as a biosensor such as high quality factor, high interaction between light and analyte and the capability for multiple detection of several bio-targets at the same time. It can be used to detect NCI-H358 lung cancer cells. As another design, a micro-cavity in a PC waveguide is presented and fabricated for detecting human IgG (Immunoglobin-G) concentration in Ref. 26. A quality factor of 500 and a sensitivity approximately equal to 0.5125 nm (red shift) per 10 $\mu g.ml^{-1}$ are reported based on experimental results. An interesting approach is used to detect IgG in Ref. 27. In addition to sensitivity, binding kinetic parameters (association and dissociation) are extracted based on experimental data. Furthermore, a very sensitive biosensor with a high quality factor is fabricated and reported in Ref. 28. The structure uses a hexagonal lattice with a slotted waveguide which makes it ultra-sensitive to the variation of refractive index. A sensitivity of 1500 nm/RIU is reported for this structure. A nanostructure PC waveguide with L3 cavity is reported in Ref. 29. The cavity is formed by removing 3 holes in a row between two waveguides. The maximum quality factors obtained in this case

* Corresponding author.
E-mail address: danaie@semnan.ac.ir (M. Danaie).

https://doi.org/10.1016/j.opelre.2019.11.007
1230-3402/

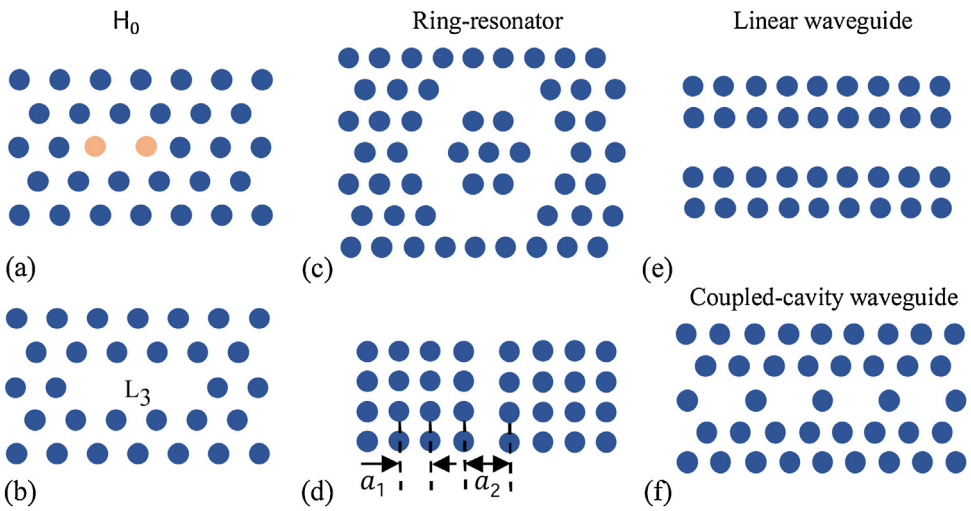

Fig. 1. Various point defects. (a) H0-cavity. (b) L3-cavity. (c) Ring resonator. (d) Hetro-structure cavity. (e) Linear waveguide. (f) Coupled-cavity waveguide.

are 2995 and 5151 (based on experimental results for different bio-targets). The reported sensitivity for the mentioned structure is 26.6 nm/pg for bovine serum albumin (BSA). Another structure has been reported in Ref. 30 which possesses a sensitivity of 160 nm/RIU and a minimal detection limit of 8.75 10^{-5} RIU. In Ref. 31 Bloch surface waves in one-dimensional PC are used to enhance and confine electromagnetic fields near the boundaries which can improve the sensing properties. Such an approach is used for the detection of clinical levels of the angiogenic factor Ang2 in patient plasma samples.

In this paper, we have tried to provide a higher sensitivity to refractive index variations, a wider detection limit and a higher quality factor by incorporating ring shaped resonators inside PCs. We have also tried to obtain the optimum design parameters using particle swarm optimization (PSO) method. A record figure of merit (FoM) of 737 RIU^{-1} is obtained for the proposed structure. The rest of this paper is organized as follows: Section 2 describes the theory behind photonic crystal biosensors. System components and detection procedure of optical label-free biosensors are explained in Section 3. Details of the designed structure are explained in Section 4. In Section 5 materials and calculation methods are described. The simulation results are presented in Section 6. We will also have a conclusions' section.

2. Photonic crystal resonators

PC structures have behaviors analogous to crystals in electrical devices. There are some forbidden frequencies or wavelengths for light propagation in PC structures which are called photonic bandgaps (PBG). This behavior originates from dispersion feature of PCs which can be modeled by Kramers-Kronig relation [32,33]. As a result, an incident electromagnetic wave whose resonant wavelength lies within the PBG will be reflected completely by the PC. Depending on the structure, a PC may have a complete PBG in one or all propagation directions. PC structures are usually categorized as one, two and three-dimensional structures [34,35]. The two-dimensional PC structure is usually chosen for most of applications.

In order to use PCs to control light for the intended applications, it is required to introduce defects to the regular lattice to create waveguides or resonators. A defect in a perfect PC lattice may create a single resonance in the bandgap region and usually creates a micro-cavity [36]. Cavities are suitable choices for sensing applications if the transmission peaks or dips are sensitive to slight changes in refractive index of the defect region. Some of common defect types for PC lattices are listed here [36,37]:

a) Hm-type: By removing m points to create a small space in the lattice. H0-cavity is created by just modifying the radius of some holes or rods without removing any point [38–40]. Figure 1 (a) shows this kind of cavity.
b) Ln-typed: By removing some lattice points in one line to form a cavity. Where, "n" is the number of removed lattice points [4], [7] [See Fig. 1(b)].
c) Ring-shaped: By removing some lattice points to form one or more ring-shaped defects and generating some localized optical modes that resonate in these rings [41–44]. [See Fig. 1(c)]
d) Hetero-structure: As seen in Fig. 1(d), changing the lattice constants, holes sizes, holes locations, or shapes of a large number of lattice points to generate resonant modes [45].
e) Single line waveguide: created by removing a complete line of lattice point [4] [Fig. 1(e)].
f) Coupled cavity waveguide (CCW): Created by coupling resonators together [36] [Fig. 1(f)].

3. Biosensors

A biosensor is an instrument consisting of two basic parts, bio-receptor and transducer. Bio-receptor is a biological molecule which can bind to the analyte (bio-target) chemically. The transducer is either a physical, piezoelectric, thermal, electrochemical, acoustic or optical device which is able to transform the signal from the interaction of analyte and receptor into a measurable signal [46–48].

3.1. Diagnostic procedure.

Practically, interaction between the analyte and corresponding receptor which is located on the structure's surface results in a refractive index. If there exists a high quality factor cavity, since the electric field is strongly confined, changes in the local refractive index will result in a considerable shift in the position of the localized mode [49]. A small dielectric constant (ε) perturbation results in resonance wavelength variation. Based on perturbation

theory, the angular frequency shift can be obtained from Eq. (1) [49]:

$$\Delta\omega_n = -\frac{\omega_n}{2}\cdot\frac{\langle E_n|\Delta\varepsilon|E_n\rangle}{\langle E_n|\varepsilon|E_n\rangle}. \quad (1)$$

where, E_n is the nth component of electric field in the cavity region (filled by an analyte). The second part in right side of the equation is usually called the filling fraction (f). The filling fraction is defined in Eq. (2). It models the overlap between the resonance field and analyte material in cavity region. A higher f corresponds to more field confinement and more sensitivity [49–51]. It is obvious that $0< f<1$:

$$f = \frac{\langle E_n|\Delta\varepsilon|E_n\rangle}{\langle E_n|\varepsilon|E_n\rangle}. \quad (2)$$

3.2. Characteristic parameters of an optical biosensor

There are some numerical and measurable properties for a refractive index sensor which can demonstrate their quality. Here we are going to review some of them.

3.2.1. Sensitivity

Two types of definitions are mostly used for photonic crystal sensors in the literature. For some structures the intensity of transmission changes when an analyte is introduced [51–53]. For such structures the sensitivity is defined as Eq. (3):

$$S = \frac{\Delta I}{\Delta n}\left(\frac{dB}{RIU}\right). \quad (3)$$

Another sensitivity definition is used for sensors which experience a resonance wavelength shift for different refractive indexes. Assuming that the chemical interaction of analyte and bio-receptor results in a change in refractive index denoted by Δn and assuming that for a constant n, $\Delta\varepsilon \approx 2n\Delta n$, then the sensitivity can be defined as Eq. (4) [54]:

$$S = \frac{\Delta\lambda}{\Delta n} = f.\frac{\lambda}{n}\left(\frac{nm}{RIU}\right). \quad (4)$$

The sensitivity can also be defined in nm/dl [See Eq. (5)]. Here, n is the refractive index and C is the concentration of bio-target in the sample. Usually, there is a direct relationship between concentration of a bio-target in the sample and the index of refraction [55,56]. When concentration is increased, the refractive index increases too:

$$S\left(\frac{nm}{dl}\right) = \frac{\Delta\lambda}{\Delta n}\left(\frac{nm}{RIU}\right)\times\frac{\Delta n}{\Delta C} = \frac{\Delta\lambda}{\Delta C}. \quad (5)$$

For some materials, $\Delta n/\Delta C$ is constant. Some measurement results are reported for refractive indices of hemoglobin, amino acids and proteins for different concentrations and wavelengths in [55–58].

3.2.2. Quality factor

The quality factor which is defined as the ratio of the resonance wavelength to the bandwidth measured at full width half maximum (FWHM) is a parameter which models the field confinement in a cavity. To have a higher sensitivity, the quality factor needs to be as high as possible. Equation (5). defines the quality factor [54]:

$$Q = \frac{\lambda(\text{resonance})}{\Delta\lambda(\text{FWHM})}\ (\text{unit-less}). \quad (6)$$

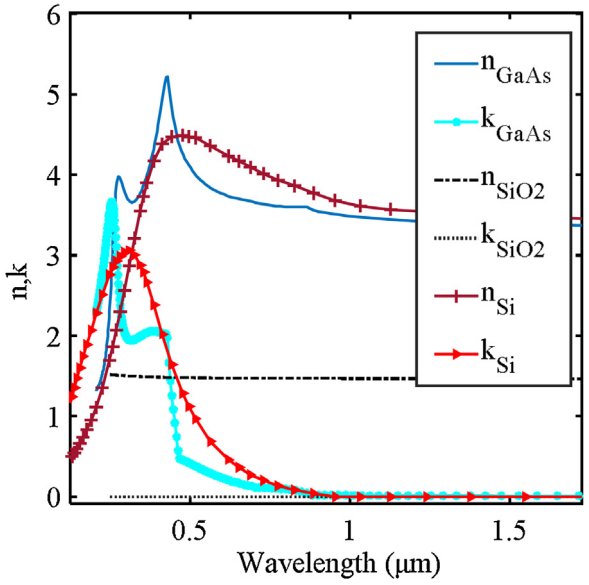

Fig. 2. The refractive index diagrams for SiO_2, Si and GaAs.

3.2.3. Minimum detection limit

The detection limit (DL) is defined based on product of quality factor and sensitivity [28], [54]:

$$DL = K\frac{\omega_0}{QS}\ (RIU). \quad (7)$$

where, K is the proportionality constant. It is based on the spectral line shape and signal-to-noise ratio (SNR) of the measurement system. Consequently, to have a good biosensor a small DL is required.

3.2.4. Figure of merit

To compare performance of biosensors, having a well-defined figure of merit (FoM) is the key parameter. It is usually defined by dividing the sensitivity of the biosensor to its FWHM bandwidth [59,60 [See Eq. (8)]:

$$FoM = \frac{S}{\Delta\lambda_{FWHM}}\ (RIU^{-1}). \quad (8)$$

4. Material and calculation method

4.1. Material properties

For absorbing materials, the refractive index is modelled in a complex format as Eq. (9). Where, n and k are the real and imaginary parts of the complex refractive index [61,62]. The refractive indices of the materials used here are shown in Fig. 2 .

$$n = \sqrt{\mu\varepsilon} = n(\omega) - ik(\omega). \quad (9)$$

The imaginary part (k) is called the absorption coefficient of the medium. If $k > 0$, then there is absorption and if $k < 0$, then there is optical amplification in the system. For sensing applications, a zero absorption for structure's material is preferred. If a part of field energy is absorbed by the composing material, the sensor efficiency may be decreased. For this purpose, materials with zero absorption in working wavelengths are selected. Here, GaAs is used for the rods of the PC. For lower index substrate SiO_2 is selected. We chose SiO_2 for its minimum absorption in working wavelengths. For that purpose, we have used the model shown in Fig. 3 which compares Si, GaAs and SiO_2 [61–63]. For this purpose, the refractive indices are extracted from [64,65].

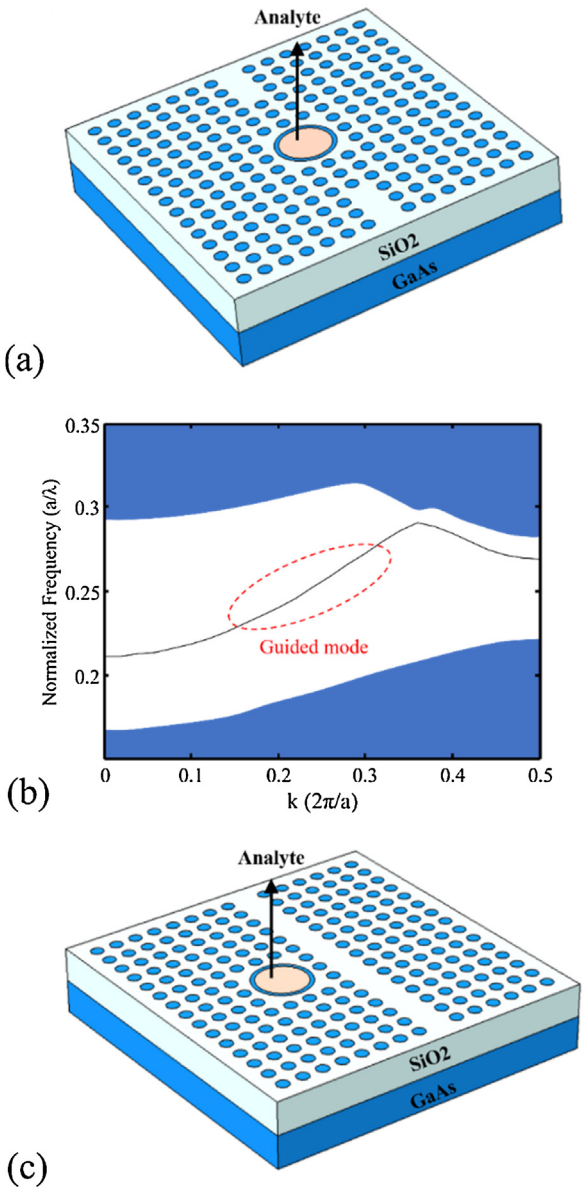

Fig. 3. (a) The first proposed biosensor. (b) The band structure and guided mode for the first structure's waveguide. (c) The second proposed topology based on a side-coupled cavity.

4.2. Calculation methods

Finite deference time domain (FDTD), plane wave expansion (PWE) and particle swarm optimization (PSO) methods are used to calculate the transmission spectrum, band structures and optimum parameter of designed biosensor, respectively. PSO is a well-known algorithm which was developed by Eberhart and Kennedy in 1995 [54,55]. Details of calculation methods for FDTD and PWE are explained in Refs. 62, 66 and 36. The PSO algorithm is exhaustively explained in Refs. 67 and 68.

5. Biosensor design

In this paper, two photonic crystal structures are designed and simulated. The first structure is presented in Fig. 3(a). As can be seen, cavities are ring-shaped defects accompanied by three rods in each side of the ring. The rod's radii are optimized for the maximum transmission. A lattice constant equal to a = 390 nm and a rod radius of r = 0.3a are selected to have a photonic band gap in the normalized frequency range of 0.2253 a/ λ to 0.265 a/ λ for transverse magnetic (TM) modes. The band structure for the guided mode is presented in Fig. 3(b). The optimum amounts of radii are selected using PSO algorithm. The additional rods have a radius equal to $r_h = 0.34a$. The inner radius of the ring is $r_i = 1.2a$ and the outer radius is $r_o = 1.4a$. As seen in Fig. 3(c), for the second structure the ring-shaped cavity is side-coupled to the waveguide. The structures have nearly a 1 μm^2 sensitive area. Such a feature makes them suitable for integration and especially for lab on chip applications. To inject samples into the structure, microfluidic channels can be employed and integrated with the biosensor. The details of fabrication and integration process needed in such a case have presented in Refs. 67–69 (See Fig. 4).

6. Simulation results and discussion

6.1. Ring-shape cavity coupled to waveguides

When the analyte is water (with a refractive index of 1.33), the structure acts as a very narrow-band bandpass filter which reflects all wavelengths except 1525 nm with a 97.8 % transmittance. There is a tradeoff between maximum transmission, sensitivity and quality factor. A 97.8 % transmission peak, 739 nm/RIU sensitivity and quality factor of 1256 are obtained. The sensitivity is optimized by maximization of filing fraction which was mentioned in Eq. (2) for an analyte refractive index of 1.35 at 1.545 μm. The FWHM bandwidth is 1.003 nm. As a result of Eq. (8), FoM is 734 RIU^{-1} which is significantly high. Figure 5(a) presents the top-view of designed structure. The vertical component of the electric field is depicted in Fig. 5(b). As seen, the structure shows a good performance in field confinement. The simulation results for different analyte refractive indices are presented in Fig. 6(a). A 7.39 nm resonance wavelength shift is observed when the refractive index of the cavity is changed from 1.35 to 1.36 which results in a 739 nm/RIU sensitivity. From the simulation results, the sensitivity of the design is maximum when refractive index of analyte changes from 1.35 to 1.36. The detection limit can be calculated using Eq. (7). The detection limit for this structure is in order of 10^{-4} RIU. Also, the wide range of detectable refractive indices of this structure makes it desirable for detecting a wide range of concentrations for various analytes.

In order to observe the sensitivity of sensor, resonance wavelength vs refractive index of analyte is plotted in Fig. 5(b). According to this graph, the relationship between the analyte refractive index and the resonance wavelength is almost linear. The sensitivity of the sensor, which is equal to the slope of the graph, is approximately constant and it is equal to 739 nm/RIU.

The outer radius of ring is swept to demonstrate how the maximum transmission and the filling fraction change. To illustrate the effect of r_h variation on transmission behavior and sensitivity of the structure, transmission and filling fraction are calculated for different amounts of r_h and the results are presented in Fig. 6. For much smaller radii than the optimum amount of r_h, the transmission peak is very weak. By increasing the radius of mentioned rods, the peak of transmission gradually becomes better. After that, the transmission behavior changes and the high-quality resonance peak disappears [See Fig. 6(a)]. As can be seen from Fig. 6(b), at first, the maximum filling fraction has a slight increment but later it decreases with a fairly large slope.

6.1.1. Replacing GaAs with Si

Using Si instead of GaAs seems to be an interesting suggestion for two reasons. First, it results in a lower fabrication cost and secondly SiO_2 which is used as the low index photonic crystal material has good compatibility with Si. We have repeated our simulation for

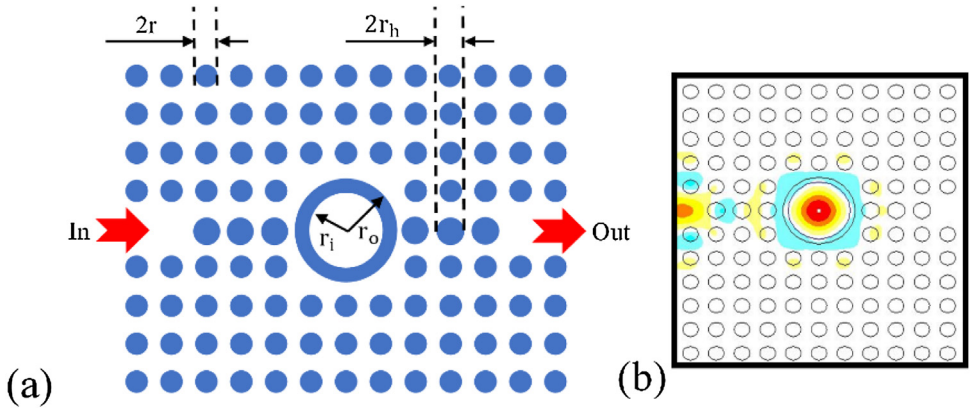

Fig. 4. (a) Top view of first proposed structure with a = 390 nm, r = 0.3a, r_i = 1.2a, r_o = 1.4a, r_h = 0.34a. (b) The resonance profile of the strucutre.

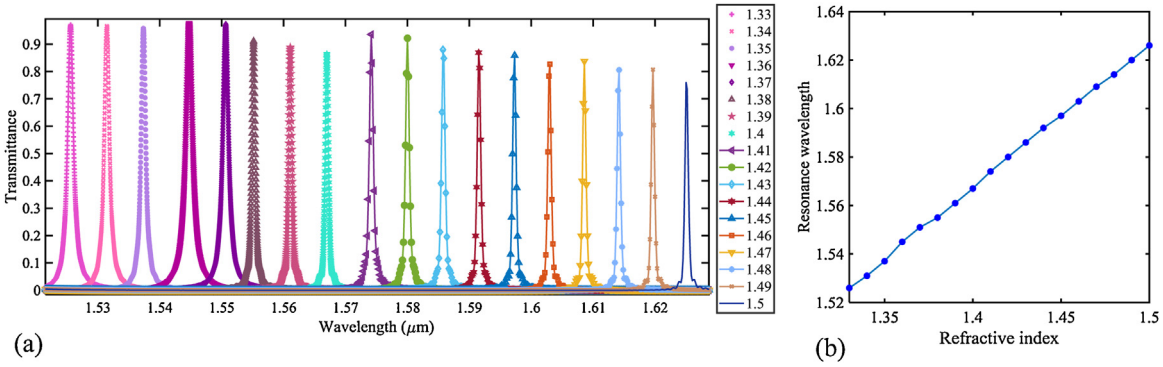

Fig. 5. (a) Transmission spectrum of structure, (b) Resonance wavelength of 2D PC in terms of analyte refractive index.

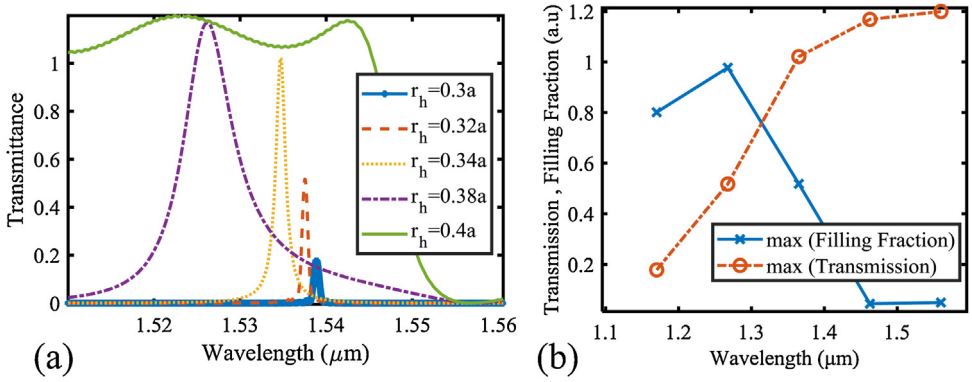

Fig. 6. (a) Transmission spectrum for different radii of cavity rods in waveguide. (b) The maximum transmission and filling fraction.

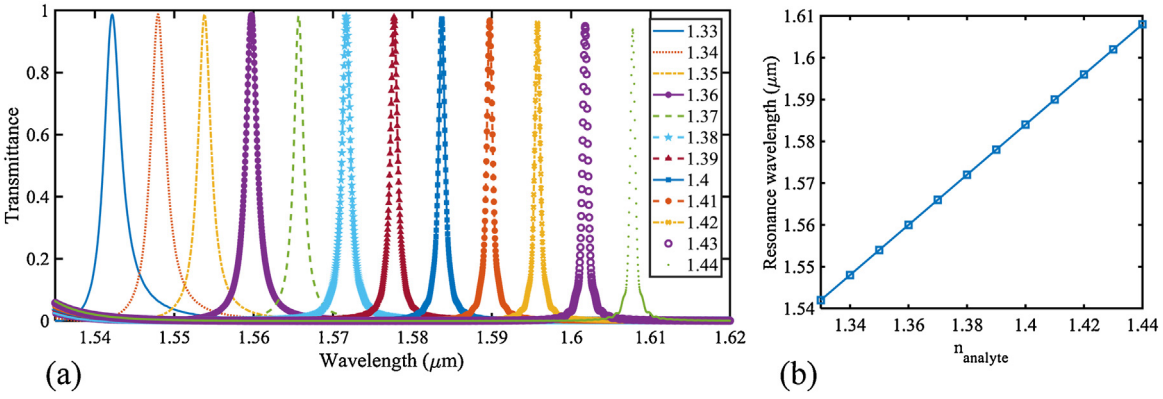

Fig. 7. (a) Transmission spectrum of structure when Si is used instead of GaAs, (b) Resonance wavelength of in terms of analyte refractive index for such a case.

the case when GaAs is replaced by Si. The transmission spectrum in such a case for different values of analyte refractive indices is depicted in Fig. 7(a). As seen distinct resonance peaks are observed in the such as case. It means that the same topology works for Si. However, comparing the results with those depicted in Fig. 5(a) show that narrower transmission spectra are observed for GaAs. As an example, for analytes with a refractive index of 1.33, the quality factor calculated for Si is equal to 616. The sensitivity is approximately 600 nmRIU^{-1} and the FoM is 240 RIU^{-1}. Although these values are relatively good, but they are lower than GaAs results. Consequently, the designer can also employ Si for design of the sensor and enjoy the benefits associated with Si, while having a slightly lower resolution compared to GaAs.

6.2. Side-coupled ring cavity

The top view of the second designed PC biosensor structure is presented in Fig. 8(a). It has similar parameters with the previous design, where a = 390 nm, r_i = 1.2a, r_o = 1.4a, and r = 0.3a. The vertical component of the electrical field is presented in Fig. 8(b). The field is confined and resonates inside the cavity region. As Figure 8(c) shows, the cavity with 2a distance from center of waveguide, is a narrow-band notch filter which has a sensitive dip in 1529 nm and a quality factor equal to 301 for when the analyte refractive index is 1.35 RIU. When the analyte refractive index is changed from 1.35 to 1.36, a 5.36 nm wavelength shift observed. Consequently, the sensitivity is 536 nm/RIU and the minimum detection limit is 9.5 $\times$ 10^{-4}. The simulations are repeated for two other different coupling distances (y_r) and the results are summarized in Fig. 9. For y_r =3a, a resonance dip is observed in 1533 nm for an analyte refractive index of 1.35. A quality factor of 1231 and a bandwidth of 1.23 nm are also observed. The resonance wavelength shifts from 1533 nm to 1539 nm when refractive index of cavity is changed to 1.36 RIU which results in a 600 nm/RIU sensitivity. The FoM is 487 RIU^{-1} for such a case. Likewise, for y_r = 4a, a resonance dip is found in 1534 nm for an analyte with a refractive index equal to 1.35. The bandwidth is 1.4 nm and the quality factor is 1096. When the refractive index of cavity changes to 1.36, a wavelength shift of 6 nm occurs. Consequently, the sensitivity of this design is 600 nm/RIU and FoM is 428 RIU^{-1}. The results for y_r = 4a do not show improvement in comparison with y_r = 3a.

As seen in Fig. 8(c), a considerable variation is seen in transmittance curves for a 0.01 variation in the refractive index. The reason behind such a huge variation can be explained using the field profile pattern in Fig. 8(b) and Eq. (1). The maximum intensity of the resonance profile is located inside the ring which is filled with the analyte. According to Eq. (1), the change in the resonance frequency depends on total sum of the product of electrical field intensity and $\Delta\varepsilon$. Since the biggest portion of the energy is stored inside the ring, the value of the numerator of the fraction is increased for the proposed cavity. In simple words, for resonators that exhibit a resonance profile which is exactly located on analyte, a high sensitivity to refractive index variation is expected.

6.3. Results and comparisons

Some of the best recent photonic crystal biosensor structures are listed in Table 1. Where, ppm (part per million) is concentration unit of analyte in very low-density solutions. Also, fg (femtogram) and pg (picogram) are unit of mass which are 10^{-15} and 10^{-12} gram, respectively. M is molar density of molecules. The structures are

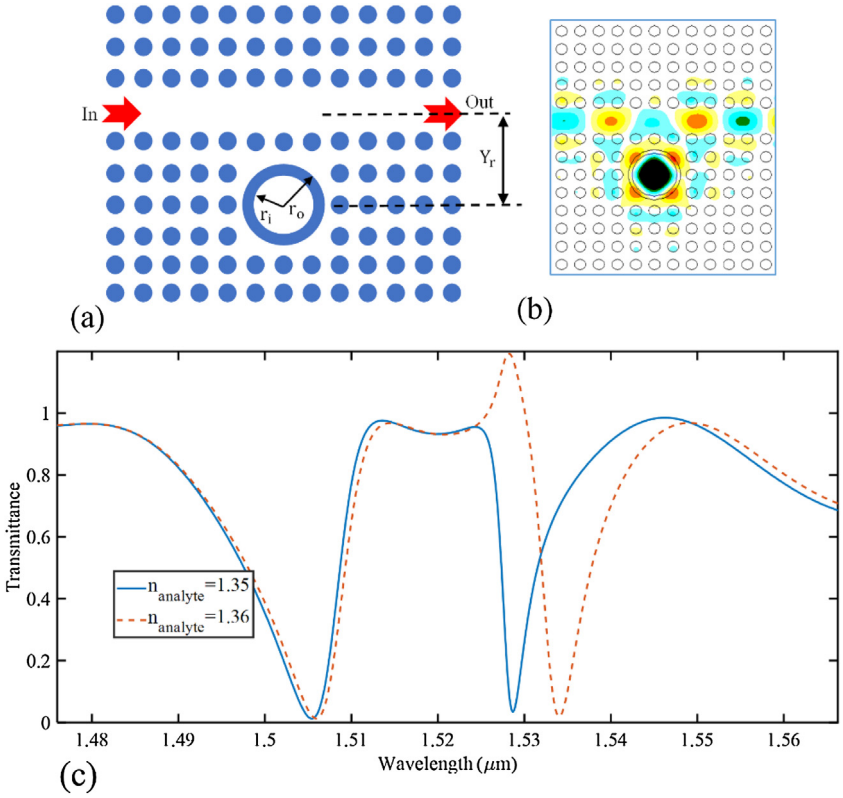

Fig. 8. (a) Top view of the designed side-couple cavity biosensor for yr = 2a. (b) The vertical component of electric field confined in cavity region. (c) The transmission spectrum for different analyte refractive indices.

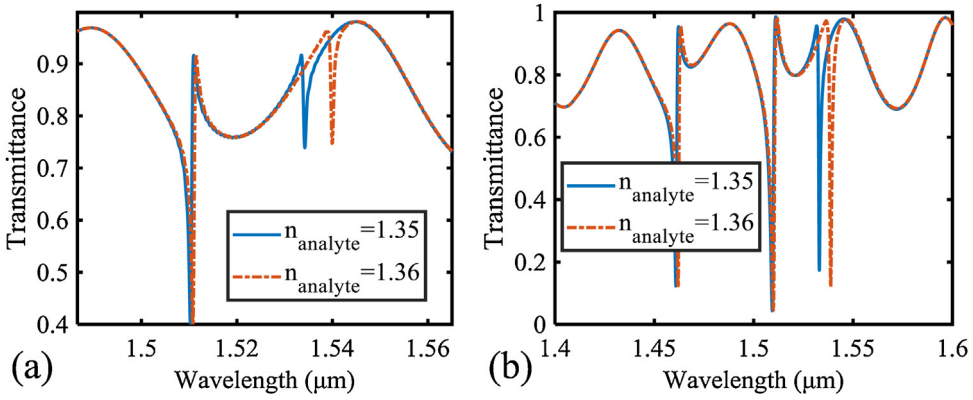

Fig. 9. (a) Transmission and wavelength shift for the coupling length of 3a. (b) The transmission spectrum and wavelength shift for a coupling length equal to 4a.

Table 1
Comparison between different bio-sensors and the current work.

Reference	Year	Detection target	structure	Quality factor	sensitivity	Detection limit	Figure of merit (RIU^{-1})	Fabrication/ measurement
[13]	2018	cancer	Ring-shape	25-30	638-720 nm/RIU	6.25×10^{-3}	–	No
[15]	2012	cancer	L13	7000	66 nm/RIU	–	–	Yes
[26]	2011	protein	Point defect	500	2.3×10^{-5} nm/M	1.5fg	–	Yes
[70]	2015	—	Tooth-shaped stubs	–	1060	–	176.7	No
[71]	2009	Caster sugar	Hetro-type	4000	1538 nm/RIU	7.8×10^{-6} RIU	–	Yes
[72]	2014	–	Shoulder-coupled	15000	141.67 nm/RIU	–	–	No
[73]	2018	VEGF biomarker	One-dimensional PC	–	–	11 ng/mL	–	Yes
[74]	2015	–	H0 and H1	2480	620 nm/RIU	9.4322 ppm	–	No
[75]	2012	–	Half-ring	950	293 nm/RIU	–	–	No
[76]	2011	–	Hm	2761	115.6 nm/RIU	8.65×10^{-5} RIU	–	No
[77]	2009	–	L3	–	24.7 nm/pg	4.0fg	–	Yes
[78]	2007	Single particle	Point defect	2000	4nm redshift for captured particle	–	–	No
[79]	2016	glucose	Cavity- waveguide	269	–	–	–	No
[80]	2010	Molecule binding	One-dimensional PC		1840 nm/RIU	10^{-8} RIU	–	Yes
[81]	2017	ERBB2 in breast cancer cell	One-dimensional PC	–	–	10 pM	–	Yes
[82]	2011	biomarkers	PC polymer array	7500	0.129 pm/(pg/mm^2)	8 pg/mm^2	–	Yes
[83]	2015	protein	Ring resonator	–	40 nm/RIU	–	–	No
[84]	2015		Nano-ring	3700	3.4 nm/fg	0.029 fg	–	No
[85]	2015	Refractive index	Plasmonic side-coupled cavity	–	1562 nm/RIU	–	38.6	No
[86]	2016	Refractive index	Plasmonic ring resonator	–	985 nm/RIU	–	28.5	No
[87]	2017	Refractive index	Plasmonic ring resonator		1125 nm/RIU	–	75	No
[88]	2018	Refractive index	plasmonicNano-rods	–	1587 nm/RIU	–	6.1	Yes
[89]	2018	Refractive index	Plasmonic Concentric Ring Resonators	–	1060 nm/RIU	–	203	No
Current work	2018	Refractive index	ring cavity with rods in waveguide	1256	739 nm/RIU	1.6×10^{-4} RIU	737	No
		Refractive index	Side-coupled ring	1432-2081	536-600 nm/RIU	1.24×10^{-4} RIU	487	No

compared based on different performance metrics. The question that "which biosensor feature has the most importance" depends on the way and where it is going to be used. The figure of merit is the most important biosensor parameter for comparing structures and technologies. The proposed structure is able to compete with plasmonic structures in terms of sensitivity and FoM parameters.

The biosensor structures which are designed in this work are able to detect most of refractive indices which are required for bio-sensing applications. As seen the highest FoM belongs to the proposed structures.

7. Conclusions

Two photonic crystal refractive index sensor structures were designed and proposed in this paper. The structures were based on square lattice of GaAs rods. The sensors were numerically simulated using finite difference time domain method. The first design was a narrow-band filter which had maximum sensitivity, quality factor, and minimum detection limit of 739 nm/RIU, 1256, and 1.6×10^{-4} RIU, respectively. The second one is a notch filter which reflects the resonance wavelength near the 1530 nm completely. A record FoM value of 737 RIU^{-1} was calculated in this paper. The

structures proposed in these papers are good candidates for lab on chip applications.

Author agreement statement

We the undersigned declare that this manuscript is original has not been published before and is not currently being considered for publication elsewhere. We confirm that the manuscript has been read and approved by all named authors and that there are no other persons who satisfied the criteria for authorship but are not listed. We further confirm that the order of authors listed in the manuscript has been approved by all of us. We understand that the Corresponding Author is the sole contact for the editorial process. He is responsible for communicating with the other authors about progress, submissions of revisions and final approval of proofs signed by all authors.

References

[1] E. Kuramochi, H. Duprez, J. Kim, M. Takiguchi, K. Takeda, T. Fujii, K. Nozaki, A. Shinya, H. Sumikura, K. Taniyama, S. Matsuo, M. Notomi, Room temperature continuous-wave nanolaser diode utilized by ultrahigh-Q few-cell photonic crystal nanocavities, Opt. Express 26 (2018) 26598–26617.
[2] T. Watanabe, Y. Saijo, Y. Hasegawa, K. Watanabe, Y. Nishijima, T. Baba, Ion-sensitive photonic-crystal nanolaser sensors, Opt. Express 25 (2017) 24469–24479.
[3] M. Danaie, H. Kaatuzian, Design of a photonic crystal differential phase comparator for a Mach–Zehnder switch, J. Opt. 13 (2010), 015504.
[4] A. Salmanpour, S. Mohammadnejad, A. Bahrami, Photonic crystal logic gates: an overview, Opt. Quant. Electron. 47 (2015) 2249.
[5] M. Danaie, H. Kaatuzian, Design and simulation of an all-optical photonic crystal AND gate using nonlinear Kerr effect, Opt. Quant. Electron. 44 (2012) 27–34.
[6] V.S. Amaratunga, T.H. Hattori, M.H. Premaratne, H. Tan, C. Jagadish, Photonic crystal phase detector, J. Opt. Soc. Am. B 25 (2008) 1532–1536.
[7] B. Momeni, E. Shah Hosseini, M. Askari, M. Soltaniand, A. Adibi, Integrated photonic crystal spectrometers for sensing applications, Opt. Commun. 282 (2009) 3168–3171.
[8] M. Danaie, H. Kaatuzian, Improvement of power coupling in a nonlinear photonic crystal directional coupler switch, Photon. Nanostruct.: Fundam. Appl. 9 (2011) 70–81.
[9] N. Yamamoto, T. Ogawa, K. Komori, Photonic crystal directional coupler switch with small switching length and wide bandwidth, Opt. Express 14 (2006) 1223–1229.
[10] A. Ghaffari, M. Djavid, F. Monifi, M.S. Abrishamian, Photonic crystal power splitter and wavelength multi/demultiplexer based on directional coupling, J. Opt. A: Pure Appl. Opt. 10 (7) (2008), 075203.
[11] M. Danaie, R. Nasiri Far, A. Dideban, Design of a high-bandwidth Y-shaped photonic crystal power splitter for TE modes, Int. J. Opt. Photon. (IJOP) 12 (2018) 33–42.
[12] K. Zhang, L.B. Zhao, S.S. Guo, B.X. Shi, T.L. Lam, Y.C. Leung, Y. Chen, X.Z. Zhao, H.L. Chan, Y. Wang, A microfluidic system with surface modified piezoelectric sensor for trapping and detection of cancer cells, Biosens. Bioelectron. 26 (2) (2010) 935–939.
[13] X. Yu, B. Munge, V. Patel, G. Jensen, A. Bhirde, J.D. Gong, S.N. Kim, J. Gillespie, J.S. Gutkind, F. Papadimitrakopoulos, J.F. Rusling, Carbon nanotube amplification strategies for highly sensitive immunodetection of cancer biomarkers, J. Am. Chem. Soc. 128 (34) (2006) 11199–11205.
[14] L. Tian, K. Qian, J. Qi, Q. Liu, C. Yao, W. Song, Y. Wang, Gold nanoparticles superlattices assembly for electrochemical biosensor detection of microRNA-21, Biosens. Bioelectron. 15 (2018) 564–570.
[15] C. Justino, A.C. Duarte, T.A. Rocha-Santos, Review of analytical figures of merit of sensors and biosensors in clinical applications, Trends Analyt. Chem. 29 (10) (2010) 1172–1183.
[16] S. Khani, M. Danaie, P. Rezaei, Size reduction of MIM surface plasmon based optical bandpass filters by the introduction of arrays of silver nano-rods, Physica E: Low-dimen. Sys. Nanostruct. 113 (2019) 25–34.
[17] Y. Zhang, Y. Kuang, Z. Zhang, Y. Tang, J. Han, R. Wang, W. Liu, High-sensitivity refractive index sensors based on Fano resonance in the plasmonic system of splitting ring cavity-coupled MIM waveguide with tooth cavity, Appl. Phys. A 125 (1) (2019) 13.
[18] S. Khani, M. Danaie, P. Rezaei, Double and triple-wavelength plasmonic demultiplexers based on improved circular nanodisk resonators, Opt. Eng. 57 (10) (2018) 107102.
[19] M. Danaie, A. Geravand, Design of low-cross-talk metal–insulator–metal plasmonic waveguide intersections based on proposed cross-shaped resonators, J. Nanophotonics 12 (4) (2018) 046009.
[20] D. Liu, J. Wang, F. Zhang, Y. Pan, J. Lu, X. Ni, Tunable plasmonic band-pass filter with dual side-coupled circular ring resonators, Sensors 17 (3) (2017) 585.
[21] S. Khani, M. Danaie, P. Rezaei, Tunable single-mode bandpass filter based on metal–insulator–metal plasmonic coupled U-shaped cavities, IET Opt. 13 (4) (2019) 161–171.
[22] M. Danaie, A. Shahzadi, Design of a high-resolution metal–Insulator–Metal plasmonic refractive index sensor based on a ring-shaped Si resonator, Plasmonics 14 (6) (2019) 1453–1465.
[23] S. Khani, M. Danaie, P. Rezaei, Design of a single-mode plasmonic bandpass filter using a hexagonal resonator coupled to graded-stub waveguides, Plasmonics 14 (1) (2019) 53–62.
[24] E. Danaee, A. Geravand, M. Danaie, Wide-band low cross-talk photonic crystal waveguide intersections using self-collimation phenomenon, Opt. Commun. 431 (2019) 216–228.
[25] A. Geravand, M. Danaie, S. Mohammadi, All-optical photonic crystal memory cells based on cavities with a dual-argument hysteresis feature, Opt. Commun. 430 (2019) 323–335.
[26] M. Danaie, B. Kiani, Design of a label-free photonic crystal refractive index sensor for biomedical applications, Photon. Nanostruct.: Fundam. Appl. 31 (2018) 89–98.
[27] V. Toccafondo, J. García-Rupérez, M.J. Bañuls, A. Griol, J.G. Castelló, S. Peransi-Llopis, A. Maquieira, Single-strand DNA detection using a planar photonic-crystal-waveguide-based sensor, Opt. Lett. 35 (21) (2010) 3673.
[28] S. Chakravarty, W.C. Lai, Y. Zou, H.A. Drabkin, R.M. Gemmill, G.R. Simon, et al., Multiplexed specific label-free detection of NCI-H358 lung cancer cell line lysates with silicon based photonic crystal microcavity biosensors, Biosens. Bioelectron. 43 (2013) 50–55.
[29] S. Pal, E. Guillermain, R. Sriram, B.L. Miller, P.M. Fauchet, Silicon photonic crystal nanocavity-coupled waveguides for error-corrected optical biosensing, Biosens. Bioelectron. 26 (10) (2011) 4024–4031.
[30] A. Sinibaldi, A. Occhicone, P. Munzert, N. Danz, F. Sonntag, F. Michelotti, Label-free monitoring of human IgG/Anti-IgG recognition using bloch surface waves on 1D photonic crystals, Biosensors. 8 (2018) 71.
[31] M.G. Scullion, A. Di Falco, T.F. Krauss, Slotted photonic crystal cavities with integrated microfluidics for biosensing applications, Biosens. Bioelectron. 27 (1) (2011) 101–105.
[32] D. Dorfner, T. Zabel, T. Hürlimann, N. Hauke, L. Frandsen, U. Rant, et al., Photonic crystal nanostructures for optical biosensing applications, Biosens. Bioelectron. 24 (12) (2009) 3688–3692.
[33] L. Huang, H. Tian, J. Zhou, Q. Liu, P. Zhang, Y. Ji, Label-free optical sensor by designing a high-Q photonic crystal ring–slot structure, Opt. Commun. 15 (2015) 73–77.
[34] R. Rizzo, M. Alvaro, N. Danz, L. Napione, E. Descrovi, S. Schmieder, A. Sinibaldi, S. Rana, R. Chandrawati, P. Munzert, T. Schubert, Bloch surface wave enhanced biosensor for the direct detection of Angiopoietin-2 tumor biomarker in human plasma, Biomed. Opt. Express 9 (2018) 529–542.
[35] H. Kaatuzian, Photonic Vol1 5th Printing, Amirkabir University press, 2017.
[36] H. Kaatuzian, Photonic Vol2 4th Printing, Amirkabir University press, 2018.
[37] J.D. Joannopoulos, S.G. Johnson, J.N. Winn, R. Meade, Photonic Crystal Molding the Flow of Light, 2nd ed., Princeton university press, 2007.
[38] Q. Gong, X. Hu, Photonic Crystals_ Principles and Applications-Pan, Stanford Publishing,CRC Press, 2014.
[39] S. Olyaee, A. Mohebzadeh-Bahabadi, Photonic Crystals Devices, Fibers, Sanostructures, and Sensors, Shahid rajaee Teacher Training University, 2016.
[40] Y. Zhang, Y. Zhao, T. Zhou, Q. Wu, Applications and developments of on-chip biochemical sensors based on optofluidic photonic crystal cavities, Lab Chip 18 (1) (2018) 57–74.
[41] S. Arfa, M. Bouchemat, T. Bouchemat, A. Benmerkhi, High sensitive optpfluidic sensor array based onring-shaped hoes photonic crystal H0-cavity, Optik 131 (2017) 49–57.
[42] D. Yang, H. Tian, Y. Ji, The properties of lattice-shifted microcavity in photonic crystal slab and its applications for electro-optical sensor, Sens. Actuators A Phys. 171 (2) (2011) 146–151.
[43] Y.N. Zhang, Y. Zhao, D. Wu, Q. Wang, Fiber loop ring-down refractive index sensor based on high- q photonic crystal cavity, IEEE Sens. J. 14 (6) (2014) 1878–1885.
[44] S. Robinson, K. Vijaya Shanthi, Analysis of protein concentration based on photonic crystal ring resonator, IJOP 10 (2) (2016) 123–130.
[45] R. Rajasekar, S. Robinson, Nano-pressure and temperature sensor based on hexagonal photonic crystal ring resonator, Plasmonics (2018), http://dx.doi.org/10.1007/s11468-018-0771-x.
[46] L. Hajshahvaladi, H. Kaatuzian, M. Danaie, Design of semiconductor photonic crystal double bandpass filter for CWDM sDesign and analysis of a plasmonic demultiplexer based on band-stop filters using double-nanodisk-shaped resonators, Opt. Eng. 51 (12) (2019) 391.
[47] M. Moradi, M. Danaie, A.A. Orouji, Design and analysis of an optical full-adder based on nonlinear photonic crystal ring resonators, Optik 172 (2018) 127–136.
[48] A. Di Falco, L. O'Faolain, T.F. Krauss, Chemical sensing in slotted photonic crystal heterostructure cavities, Appl. Phys. Lett. 94 (6) (2009), 063503.
[49] X. Fan, I.M. White, S.I. Shopova, H. Zhu, J.D. Suter, Y. Sun, Sensitive optical biosensors for unlabeled targets: a review, Anal. Chim. Acta 620 (1-2) (2008) 8–26.
[50] B. Bohounicky, S. Mousa, Biosensors: the new wave in cancer diagnosis, Nanotechnol. Sci. Appl. 1 (2010) 1–10, http://dx.doi.org/10.2147/NSA.S13465.
[51] S. Ghoshal, D. Mitra, S. Roy, D. Majumder, Biosensors and biochips for nanomedical applications: a review, Sensors Trans. J. 10 (2008).

[52] N.A. Mortensen, S. Xiao, J. Pedersen, Liquid-infiltrated photonic crystals: enhanced light-matter interactions for lab-on-a-chip applications, Microfluid. Nanofluidics 4 (1–2) (2007) 117–127.
[53] L. Yonghao, Z. Weidong, S. Yuze, Optical refractive index sensing based on high bound state in the continuum in free-spacecoupled photonic crystal slabs, Sensors 17 (8) (2017) 1861.
[54] S. Olyaee, A. mohebzadeh-bahabady, Two-curve-shaped biosensor using photonic crystal nano-ring resonators, J. Nanostruct. 4 (3) (2014).
[55] M. Paulsen, S. Jahns, M. Gerken, Intensity-based readout of resonant-waveguide grating biosensors: systems and nanostructures, Photon. Nanostruct.: Fundam. Appl. 26 (2017) 69–79.
[56] S. Jahns, M. Bräu, B.-O. Meyer, T. Karrock, S.B. Gutekunst, L. Blohm, et al., Handheld imaging photonic crystal biosensor for multiplexed, label-free protein detection, Biomed. Opt. Express 6 (10) (2015) 3724.
[57] S. Jindal, S. Sobti, M. Kumar, S. Sharma, M.K. Pal, Nanocavity-coupled photonic crystal waveguide as highly sensitive platform for cancer detection, IEEE Sens. J. 16 (10) (2016) 3705–3710.
[58] N.F.F. Areed, M.F.O. Hameed, S.S.A. Obayya, Highly sensitive face-shaped label-free photonic crystal refractometer for glucose concentration monitoring, Opt. Quant. Electron. 49 (1) (2017), 5, 1-12.
[59] S. Chowdhury, A. Maity, Numerical analysis of photonic crystal fiber based hemoglobin sensor, IJLEO 130 (2017) 825–829.
[60] O. Zhernovaya, O. Sydoruk, V. Tuchin, A. Douplik, The refractive index of human hemoglobin in the visible range, Phys. Med. Biol. 56 (13) (2011) 4013–4021.
[61] T.L. McMeekin, M. Wilensky, M.L. Groves, Refractive indices of proteins in relation to amino acid composition and specific volume, Biochem. Biophys. Res. Commun. 7 (2) (1962) 151–156.
[62] M.R. Rakhshani, M.A. Mansouri-Birjandi, Utilizing the metallic nano-rods in hexagonal configuration to enhance sensitivity of the plasmonic racetrack resonator in sensing application, Plasmonics 12 (4) (2016) 999–1006.
[63] L. Chen, Y. Liu, Z. Yu, D. Wu, R. Ma, Y. Zhang, H. Ye, Numerical analysis of a near-infrared plasmonic refractive index sensor with high figure of merit based on a fillet cavity, Opt. Express 24 (9) (2016) 9975.
[64] E. Palik, Handbook of Optical Constants of Solids, Elsevier, 2012, ISBN: 9780080556307.
[65] B.E.A. Saleh, M.C. Teich, Fundamental of Photonics, 2nd ed, Wiley, New York, 2007.
[66] http://refractiveindex.info.
[67] I.C. Trelea, The particle swarm optimization algorithm: convergence analysis and parameter selection, Inf. Process. Lett. 85 (6) (2003) 317–325.
[68] Y. Shi, and R. C. Eberhart, (n.d.). Empirical study of particle swarm optimization. Proc. 1999 Congress on Evolutionary Computation-CEC99 (Cat. No. 99TH8406).
[69] S. Khorasani, Introduction to Photonic Crystals Optic, Sharif university press, 2007.
[70] C.J. Choi, I.D. Block, B. Bole, D. Dralle, B.T. Cunningham, Label-free photonic crystal biosensor integrated microfluidic chip for determination of kinetic reaction rate constants, IEEE Sens. J. 9 (12) (2009) 1697–1704.
[71] C. Monat, P. Domachuk, B.J. Eggleton, Integrated optofluidics: a new river of light, Nat. Photonics 1 (2) (2007) 106–114.
[72] C.J. Choi, B.T. Cunningham, Single-step fabrication and characterization of photonic crystal biosensors with polymer microfluidic channels, Lab Chip 6 (10) (2006) 1373.
[73] R. Zafar, M. Salim, Enhanced figure of merit in Fano resonance-based plasmonic refractive index sensor, IEEE Sens. J. 15 (11) (2015) 6313–6317.
[74] A. Di Falco, L. O'Faolain, T.F. Krauss, Chemical sensing in slotted photonic crystal heterostructure cavities, Appl. Phys. Lett. 94 (6) (2009), 063503.
[75] S. Najafgholinezhad, S. Olyaee, A photonic crystal biosensor with temperature dependency investigation of micro-cavity resonator, Opt. – Int. J. Light Electron. Opt. 125 (21) (2014) 6562–6565.
[76] R. Rizzo, M. Alvaro, N. Danz, L. Napione, E. Descrovi, S. Schmieder, A. Sinibaldi, R. Chandrawati, S. Rana, P. Munzert, T. Schubert, Bloch surface wave label-free and fluorescence platform for the detection of VEGF biomarker in biological matrices, Sens. Actuators B Chem. 1 (2018) 2143–2150.
[77] Y. Zhang, Y. Zhao, H. Hu, Miniature photonic crystal cavity sensor for simultaneous measurement of liquid concentration and temperature, Sens. Actuators B-Chem. 216 (2015) 563–571.
[78] F. Hosseinibalam, S. Hassanzadeh, A. Ebnali-Heidari, C. Karnutsch, Design of an optofluidic biosensor using the slow-light effect in photonic crystal structures, Appl. Opt. 51 (5) (2012) 568.
[79] D. Yang, H. Tian, Y. Ji, Nanoscale photonic crystal sensor arrays on monolithic substrates using side-coupled resonant cavity arrays, Opt. Express 19 (21) (2011) 20023.
[80] D. Dorfner, T. Zabel, T. Hürlimann, N. Hauke, L. Frandsen, U. Rant, et al., Photonic crystal nanostructures for optical biosensing applications, Biosens. Bioelectron. 24 (12) (2009) 3688–3692.
[81] M.R. Lee, P.M. Fauchet, Nanoscale microcavity sensor for single particle detection, Opt. Lett. 32 (22) (2007) 3284.
[82] S. Robinson, N. Dhanlaksmi, Photonic crystal based biosensor for the detection of glucose concentration in urine, Photonic Sens 7 (1) (2016) 11–19.
[83] Y. Guo, J.Y. Ye, C. Divin, B. Huang, T.P. Thomas, J.R. Baker, T.B. Norris, Real-time biomolecular binding detection using a sensitive photonic crystal biosensor, Anal. Chem. 82 (12) (2010) 5211–5218.
[84] A. Sinibaldi, C. Sampaoli, N. Danz, P. Munzert, L. Sibilio, F. Sonntag, A. Occhicone, E. Falvo, E. Tremante, P. Giacomini, F. Michelotti, Detection of soluble ERBB2 in breast cancer cell lysates using a combined label-free/fluorescence platform based on Bloch surface waves, Biosens. Bioelectron. 15 (2017) 125–130.
[85] F. Dortu, H. Egger, K. Kolari, T. Haatainen, P. Furjes, Z. Fekete, et al., Design and process development of a photonic crystal polymer biosensor for point-of-care diagnostics, Biomed. Spectrosc. Imaging (2011), 80870D.
[86] M. Nikoufard, A.F. Dastjani, A. Farhadi, Photonic crystal based MZI biosensor on InP materials, 2015 23rd Iranian Conference on Electrical Engineering (2015).
[87] S. Olyaee, A.M. Bahabady, Design and optimization of diamond-shaped biosensor using photonic crystal nano-ring resonator, Opt. – Int. J. Light Electron. Opt. 126 (20) (2015) 2560–2564.
[88] Y.-Y. Xie, Y.-X. Huang, W.-L. Zhao, W.-H. Xu, C. He, A novel plasmonic sensor based on metal–insulator–metal waveguide with side-coupled hexagonal cavity, IEEE Photonics J. 7 (2) (2015) 1–12.
[89] F. Chen, D. Yao, Realizing of plasmon Fano resonance with a metal nanowall moving along MIM waveguide, Opt. Commun. 369 (2016) 72–78.